Acta Cryst. (1980). A**36**, 510–519

Multiply Bragg-Reflected Neutrons in Ideally Imperfect Crystals

BY B. GRABCEV AND A. D. STOICA

Institute of Nuclear Power Reactors, PO Box 5204, Bucharest, Romania

(*Received* 14 *July* 1979; *accepted* 24 *December* 1979)

Abstract

The solution of the general form of the integral transport equation is expanded in terms of orders of scattering. The method is applied to the analysis of multiply Bragg-reflected neutrons in mosaic crystals, making evident the vertical broadening of the reflected beam as well as the consequential neutron leakage in crystal spectrometers. A wavelength-dependent effective vertical mosaic spread of the crystal is defined as a function of the mean number of reflections. A detailed mathematical treatment is performed within the frames of an infinite-plane slab model (both in reflection and in transmission geometry) largely used in the literature in the studies of crystal reflectivity. Experimental results are also presented.

1. Introduction

The study of multiple-scattering effects in thermal-neutron scattering experiments has attracted a continued and sustained interest caused by:

(i) the necessity to make corrections for them in determining scattering laws and crystallographic form factors;

(ii) the need to make greater use of single-crystal monochromators, especially at low-to-medium-flux reactors.

Up-to-date reviews of the former aspect of the subject have been given by Sears (1975) and Becker & Coppens (1974). The latter has been treated in some detail by Werner & Arrott (1965) and by Werner, Arrott, King & Kendrick (1966).

In the present paper, we recast the general integral transport equation in an operator form, proper for expansion in terms of orders of scattering. This approach generalizes that of Werner & Arrott (1965) who set up a pair of coupled integral equations valid only for Bragg scattering.

The method is applied to the analysis of neutron monochromation by reflection on ideally imperfect crystals, both in reflection (Bacon & Lowde, 1948) and in transmission (Dietrich & Als-Nielsen, 1965) geometries.

Decomposition in terms of numbers of scatterings has enabled us to make evident the effect of vertical broadening of the neutron beam caused by multiple Bragg reflections. Under some experimental circumstances, especially at large Bragg angles, this effect could become very important, producing leakage of neutrons out of the experimental device.

Experimental results confirming the theoretical predictions are also presented.

2. General analysis in terms of orders of scattering

The neutron field is described in the present treatment by $\Phi(\mathbf{r},\mathbf{k})$, the $\mathbf{k}$ density of the neutron vectorial flux. So, the vectorial flux in $\mathbf{r}$, through a unit surface normal to $\mathbf{n}$, $F(\mathbf{r},\mathbf{n})$, is

$$F(\mathbf{r},\mathbf{n}) = \int \Phi(\mathbf{r},\mathbf{k})(\boldsymbol{\Omega}.\mathbf{n})\,\mathbf{dk}, \qquad (1)$$

where $\boldsymbol{\Omega} = \mathbf{k}/k$ and $\mathbf{dk} = k^2\,\mathrm{d}k\,\mathrm{d}\Omega$; $\mathrm{d}\Omega$ is an infinitesimal solid angle centered on $\boldsymbol{\Omega}$.

The scatterer is characterized by the following macroscopic cross sections:

μ_a = total cross section for nuclear absorption;

$\dfrac{\mathrm{d}\mu_s}{\mathbf{dk}_f}$ = differential scattering cross section;

$$\mu_s = \int \frac{\mathrm{d}\mu_s}{\mathbf{dk}_f}\,\mathbf{dk}_f = \text{total scattering cross section;}$$

where $\mathbf{k}_f$ is the wave vector of a scattered neutron.

Let us consider a convex sample of arbitrary shape (Fig. 1). Let $l_0(\mathbf{r}_0)$ be the linear coordinate of the point $A(\mathbf{r}_0)$ measured along $\mathbf{k}_0$, relative to an arbitrary origin and $l_0(\mathbf{r}_1)$ the coordinate of the point $X(\mathbf{r}_1)$ lying on $\mathbf{k}_0$. At the same time, $l_1(\mathbf{r}_1)$ is the linear coordinate of $X(\mathbf{r}_1)$ measured along a certain wave vector $\mathbf{k}_1$, intersecting $\mathbf{k}_0$ at $X(\mathbf{r}_1)$; $l_0(\mathbf{r}_{0,F})$ and $l_1(\mathbf{r}_{1,F})$ are the linear coordinates of the boundary points $B(\mathbf{r}_{0,F})$ and $C(\mathbf{r}_{1,F})$, respectively.

0567-7394/80/040510-10$01.00

The increase of the **k** density of the neutron flux at the point $l_0(\mathbf{r}_1)$ due to neutrons passing from different wave vector states $|\mathbf{k}_1\rangle$ to $|\mathbf{k}_0\rangle$ by scattering along the segment $[l_0(\mathbf{r}_1) - \mathrm{d}l_0(\mathbf{r}_1), l_0(\mathbf{r}_1)]$ is given by

$$\mathrm{d}\Phi_s[l_0(\mathbf{r}_1), \mathbf{k}_0] = \mathrm{d}l_0(\mathbf{r}_1) \int \mathbf{dk}_1 \frac{\mathrm{d}\mu_s}{\mathbf{dk}_0} \Phi[l_1(\mathbf{r}_1), \mathbf{k}_1]. \quad (2)$$

We suppose that $\mathrm{d}l_0(\mathbf{r}_1)$ is large enough to include structural and dynamical effects but, on the other hand, small enough to involve single scattering only.

Equation (2) may be rewritten,

$$\mathrm{d}\Phi_s[l_0(\mathbf{r}_1), \mathbf{k}_0] = \mathrm{d}l_0(\mathbf{r}_1) . \hat{\mathbf{S}}(\mathbf{k}_0, \mathbf{k}_1) \Phi[l_1(\mathbf{r}_1), \mathbf{k}_1],$$

where

$$\hat{\mathbf{S}}(\mathbf{k}_0, \mathbf{k}_1) = \int \mathbf{dk}_1 \frac{\mathrm{d}\mu_s}{\mathbf{dk}_0} \quad (3)$$

is the scattering operator.

The neutron group being at a certain instant of time at the point A in the $|\mathbf{k}_0\rangle$ state is composed of the neutrons entering the sample at point B in the same state and covering the space BA without interactions, to which there are added the neutrons passing from different $|\mathbf{k}_1\rangle$ states to the $|\mathbf{k}_0\rangle$ state by scattering along the line BA, afterwards being transmitted at A, *i.e.*

$$\begin{aligned}\Phi[l_0(\mathbf{r}_0), \mathbf{k}_0] = {} & \exp\{-\mu_T(\mathbf{k}_0)[l_0(\mathbf{r}_0) - l_0(\mathbf{r}_{0,F})]\} \\ & \times \Phi[l_0(\mathbf{r}_{0,F}), \mathbf{k}_0] + \int_{\mathbf{r}_{0,F}}^{\mathbf{r}_0} \mathrm{d}l_0(\mathbf{r}_1) \\ & \times \exp\{-\mu_T(\mathbf{k}_0)[l_0(\mathbf{r}_0) - l_0(\mathbf{r}_1)]\} \\ & \times \hat{\mathbf{S}}(\mathbf{k}_0, \mathbf{k}_1) \Phi[l_1(\mathbf{r}_1), \mathbf{k}_1], \end{aligned} \quad (4)$$

where

$$\mu_T(\mathbf{k}_0) = \mu_a(\mathbf{k}_0) + \mu_s(\mathbf{k}_0)$$

is the total macroscopic cross section.

Introducing the notation,

$$\chi[l_i(\mathbf{r}_i), \mathbf{k}_i] = \exp[\mu_T(\mathbf{k}_i) l_i(\mathbf{r}_i)] \Phi[l_i(\mathbf{r}_i), \mathbf{k}_i],$$

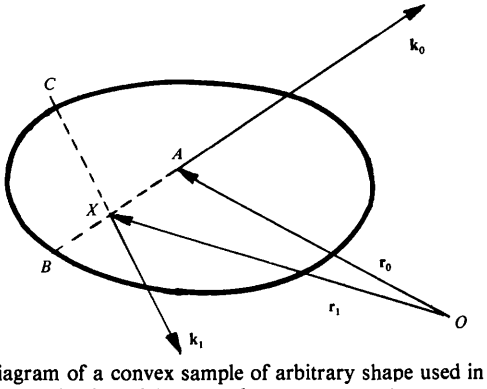

Fig. 1. Diagram of a convex sample of arbitrary shape used in the derivation of the general transport equation.

we get from (4)

$$\begin{aligned}\chi[l_0(\mathbf{r}_0), \mathbf{k}_0] = {} & \chi[l_0(\mathbf{r}_{0,F}), \mathbf{k}_0] + \int_{\mathbf{r}_{0,F}}^{\mathbf{r}_0} \mathrm{d}l_0(\mathbf{r}_1) \exp[\mu_T(\mathbf{k}_0) l_0(\mathbf{r}_1)] \hat{\mathbf{S}}(\mathbf{k}_0, \mathbf{k}_1) \\ & \times \exp[-\mu_T(\mathbf{k}_1) l_1(\mathbf{r}_1)] \chi[l_1(\mathbf{r}_1), \mathbf{k}_1]. \end{aligned} \quad (5)$$

Equation (5) may be rewritten as

$$(\hat{\mathbf{I}} - \hat{\mathbf{L}}) \chi[l_0(\mathbf{r}_0), \mathbf{k}_0] = \chi[l_0(\mathbf{r}_{0,F}), \mathbf{k}_0], \quad (6)$$

where the linear operator $\hat{\mathbf{L}}$ has the following definition:

$$\begin{aligned}\hat{\mathbf{L}} = {} & \int_{\mathbf{r}_{f,F}}^{\mathbf{r}_f} \mathrm{d}l_f(\mathbf{r}_i) \exp[\mu_T(\mathbf{k}_f) l_f(\mathbf{r}_i)] \\ & \times \hat{\mathbf{S}}(\mathbf{k}_f, \mathbf{k}_i) \exp[-\mu_T(\mathbf{k}_i) l_i(\mathbf{r}_i)]. \end{aligned} \quad (7)$$

In the above equation, i and f denote the initial and final neutron states.

Expanding the operator $(\hat{\mathbf{I}} - \hat{\mathbf{L}})^{-1}$, we find for the solution of (6)

$$\chi[l_0(\mathbf{r}_0), \mathbf{k}_0] = \sum_{n=0}^{\infty} \hat{\mathbf{L}}^n \chi[l_n(\mathbf{r}_{n,F}), \mathbf{k}_n], \quad (8)$$

where $\hat{\mathbf{L}}^n$ means n successive applications of the operator $\hat{\mathbf{L}}$.

The interpretation of (8) is straightforward: the nth term contains the contribution to neutron flux of the neutrons reaching the point A in the $|\mathbf{k}_0\rangle$ state after n successive scatterings, to say nothing about their trajectories and intermediate states. The initial states of these neutrons are described by $|\mathbf{k}_n\rangle$.

3. Multiply Bragg-reflected neutrons in ideally imperfect crystals

Later on, we shall focus our attention on multiple elastic coherent scattering, only. The 'background' caused by incoherent and/or inelastic interactions needs a separate treatment and will not be considered here. Accordingly, we shall operate with a differential scattering cross section, $\mathrm{d}\mu_B/\mathbf{dk}_f$, corresponding to Bragg scattering. At the same time, the total cross section is separated into two components:

$$\mu_T = \mu_B + \mu,$$

where μ_B is the total macroscopic elastic coherent scattering cross section while μ corresponds to all the other neutron–crystal interactions.

Fig. 2 shows a reference frame which contains in the horizontal plane the most probable wave vectors for the incoming and reflected neutron beams, $\mathbf{k}_I$ and $\mathbf{k}_F$, respectively. The **i** axis is antiparallel to the most probable orientation of a certain reciprocal vector of the crystal lattice. $(\mathbf{k}_i)$ and $(\mathbf{k}_f)$ are the projections, on

the horizontal plane of $\mathbf{k}_i$ and $\mathbf{k}_f$, the wave vectors of a certain neutron before and after reflection at a crystalline plane, the horizontal and vertical mosaic angles of which are φ and ψ. γ_i and γ_f are the corresponding horizontal divergence angles. δ_i and δ_f are the vertical divergence angles measured between $\mathbf{k}_i$ and $\mathbf{k}_f$ and their projections on the horizontal plane. θ_B is the most probable Bragg angle.

In this particular reference frame, assuming normal distribution functions, $w_H(\varphi)$ and $w_V(\psi)$, for horizontal and vertical mosaic angles, the scattering operator may be expressed (see Appendix A) as follows:

$$\hat{\mathbf{S}}(\mathbf{k}_f,\mathbf{k}_i) = \frac{Q_c}{\sqrt{2\pi}\eta_H}\frac{1}{\sqrt{8\pi}\eta_V|\sin\theta_B|} \times \int \mathrm{d}k_i\mathrm{d}\gamma_i\mathrm{d}\delta_i \exp[-(\gamma_i+\gamma_f)^2/8\eta_H^2] \times \exp[-(\delta_i-\delta_f)^2/8\eta_V^2\sin^2\theta_B]\,\delta(k_i-k_f) \times \delta(\gamma_i+\gamma_f-2\xi), \quad (9)$$

where Q_c is the well-known crystallographic quantity given in ($A7$) while η_H and η_V are the standard deviations of $w_H(\varphi)$ and $w_V(\psi)$; the variable ξ is defined in ($A9$).

Owing to $\delta(k_i-k_f)$ in the above equation, the operator $\hat{\mathbf{S}}(\mathbf{k}_f,\mathbf{k}_i)$ commutes with the exponentials in (7) and, consequently, (8) takes the following form:

$$\chi[l_0(\mathbf{r}_0),\mathbf{k}_0] = \sum_{n=0}^{\infty} T_n\hat{\mathbf{S}}^n\chi[l_n(\mathbf{r}_{n,F}),\mathbf{k}_n], \quad (10)$$

where

$$T_n = \int_{\mathbf{r}_{0,F}}^{\mathbf{r}_0} \mathrm{d}l_0(\mathbf{r}_1)\exp\{\mu_T[l_0(\mathbf{r}_1)-l_1(\mathbf{r}_1)]\} \times \int_{\mathbf{r}_{1,F}}^{\mathbf{r}_1}\mathrm{d}l_1(\mathbf{r}_2)\exp\{\mu_T[l_1(\mathbf{r}_2)-l_2(\mathbf{r}_2)]\}\ldots \times \int_{\mathbf{r}_{n-1,F}}^{\mathbf{r}_{n-1}}\mathrm{d}l_{n-1}(\mathbf{r}_n)\exp\{\mu_T[l_{n-1}(\mathbf{r}_n)-l_n(\mathbf{r}_n)]\}. \quad (11)$$

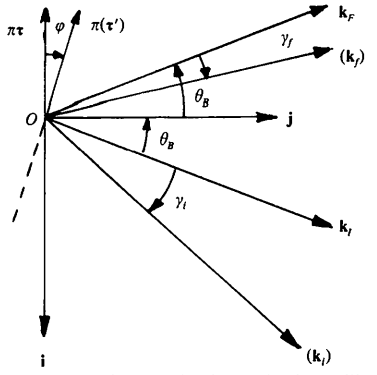

Fig. 2. Vector diagram in the horizontal plane illustrating the diffraction in a mosaic crystal.

T_n takes into account the flux changes along the zig-zag trajectories in the crystal of the n-times reflected neutrons. The remark that the total Bragg-scattering cross section is essentially different from zero only for $\mathbf{k}_i$ and $\mathbf{k}_f$ lying in narrow angular ranges around $\mathbf{k}_I$ and $\mathbf{k}_F$ [see ($A8$)] justifies the approximation in which the linear coordinates $l_i(\mathbf{r}_j)$ are measured along the most probable wave vectors.

Furthermore, the action of the function $\delta(\gamma_i+\gamma_f-2\xi)$ in (9) leads to

$$\hat{\mathbf{S}}^n(\mathbf{k}_0,\mathbf{k}_n) = \frac{\mu_B^n}{\sqrt{8\pi n}\eta_V|\sin\theta_B|}\int \mathrm{d}k_n\,\mathrm{d}\gamma_n\,\mathrm{d}\delta_n \times \exp\{-(\delta_n-\delta_0)^2/8n\eta_V^2\sin^2\theta_B\}\,\delta(k_n-k_0) \times \delta[\gamma_0+(-1)^n(\xi-\gamma_n)-\xi]. \quad (12)$$

From the above equation, it is worth noting that after an even number of reflections (transmitted beam) the horizontal divergence angle has the same value as before the first reflection. If n is odd (diffracted beam), the horizontal divergence angle is modified and correlated with the magnitude of the wave vector through ($A9$).

On the other hand, as we can see in ($A5$), the vertical component of the neutron trajectory is independent of the horizontal one as well as of the deviations of the magnitude of the wave vector from the most probable value. As a consequence, if in the incoming beam the vertical divergence angles are not correlated with the horizontal divergence angles and with the magnitude of the wave vector, we can write

$$\Phi[l_i(\mathbf{r}_i),k_i,\gamma_i,\delta_i] = \Phi[l_i(\mathbf{r}_i),k_i,\gamma_i]\,v(\delta_i) \quad (13)$$

for any value of i.

Then, the observation that according to ($A8$) μ_B is not dependent on the vertical divergence angle or mosaic spread, leads to the following equation:

$$\hat{\mathbf{S}}^{2j+1}\Phi[l_{2j+1}(\mathbf{r}_{2j+1,F}),k_{2j+1},\gamma_{2j+1}]\,v(\delta_{2j+1}) = \mu_B^{2j+1}\,\Phi[l_{2j+1}(\mathbf{r}_{2j+1,F}),k_0,2\xi-\gamma_0]\,v(\delta_0), \quad (14)$$

where

$$v(\delta_0) = \frac{1}{\sqrt{8\pi(2j+1)}\eta_V|\sin\theta_B|} \times \int \mathrm{d}\delta_{2j+1}\exp\left[-\frac{(\delta_{2j+1}-\delta_0)^2}{8(2j+1)\eta_V^2\sin^2\theta_B}\right] \times v(\delta_{2j+1}). \quad (15)$$

Furthermore, from the obvious relation

$$\int v(\delta_0)\,\mathrm{d}\delta_0 = \int v(\delta_{2j+1})\,\mathrm{d}\delta_{2j+1},$$

we conclude that even if the vertical angular distribution of neutrons could be modified by reflection, it does not influence the crystal reflectivity.

The reflectivity operator

If $\mathbf{r}_0$ is a boundary point at which the diffracted neutrons are emerging from the crystal, we write

$$\Phi[l_0(\mathbf{r}_0), k_0, \gamma_0] = \sum_{j=0}^{\infty} \Phi_{2j+1}[l_0(\mathbf{r}_0), k_0, \gamma_0],$$

where

$$\Phi_{2j+1}[l_0(\mathbf{r}_0), k_0, \gamma_0]$$

$$= \hat{\mathbf{R}}_{2j+1}\, \Phi[l_{2j+1}(\mathbf{r}_{2j+1,F}), k_{2j+1}, \gamma_{2j+1}]\, v(\delta_{2j+1})$$

is the flux density of the $(2j+1)$-times reflected neutrons.

$\hat{\mathbf{R}}_{2j+1}$ is the operator of the partial reflectivity, defined by

$$\hat{\mathbf{R}}_{2j+1} = \int \mathrm{d}\delta_0 \exp[-\mu_T l_0(\mathbf{r}_0)] \times T_{2j+1} \exp[\mu_T l_{2j+1}(\mathbf{r}_{2j+1,F})]\hat{\mathbf{S}}^{2j+1}. \quad (16)$$

It acts on the angular variables of $\Phi[l_{2j+1}(\mathbf{r}_{2j+1,F}), \mathbf{k}_{2j+1}]$ and has the proper values R_{2j+1}, *i.e.*

$$\hat{\mathbf{R}}_{2j+1}\, \Phi[l_{2j+1}(\mathbf{r}_{2j+1,F}), \mathbf{k}_{2j+1}] = R_{2j+1}\, \Phi[l_{2j+1}(\mathbf{r}_{2j+1,F}), k_0, 2\xi - \gamma_0], \quad (17)$$

where

$$R_{2j+1} = \exp[-\mu_T l_0(\mathbf{r}_0)]\, \mu_B^{2j+1} \times \exp[\mu_T l_{2j+1}(\mathbf{r}_{2j+1,F})]\, T_{2j+1}. \quad (18)$$

Through μ_B, according to (*A*8), R_{2j+1} is a function of the variable ξ.

Evidently, the operator of the total reflectivity has the following definition:

$$\hat{\mathbf{R}} = \sum_{j=0}^{\infty} \hat{\mathbf{R}}_{2j+1}. \quad (19)$$

The mean number of reflections

The mean number of reflections in the diffracted beam is defined by the following equation:

$$\langle n \rangle = \sum_{j=0}^{\infty} (2j+1) F_{2j+1}[l_0(\mathbf{r}_0), \mathbf{n}_0]/F[l_0(\mathbf{r}_0), \mathbf{n}_0], \quad (20)$$

where

$$F_{2j+1}[l_0(\mathbf{r}_0), \mathbf{n}_0] = \int \Phi_{2j+1}[l_0(\mathbf{r}_0), \mathbf{k}_0]\, (\boldsymbol{\Omega} \cdot \mathbf{n}_0)\, \mathrm{d}\mathbf{k}_0$$

according to (1) is the partial vectorial flux of the $(2j+1)$-fold reflected beam; $\mathbf{n}_0$ is parallel to the most probable direction in the emerging beam.

Assuming a uniform and collimated incoming beam, with α_0 and β_0 horizontal and vertical collimation angles, *i.e.*

$$\Phi[l_{2j+1}(\mathbf{r}_{2j+1,F}), \mathbf{k}_{2j+1}] = \Phi(k_{2j+1}) \exp(-\gamma_{2j+1}^2/2\alpha_0^2) \exp(-\delta_{2j+1}^2/2\beta_0^2),$$

we get

$$\langle n \rangle = \sum_{j=0}^{\infty} (2j+1) \int R_{2j+1}(\xi)\, \mathrm{d}\xi / \int R(\xi)\, \mathrm{d}\xi$$

$$= \sum_{j=0}^{\infty} (2j+1) I_{2j+1}, \quad (21)$$

where I_{2j+1}, the ratio of neutrons undergoing $(2j+1)$ reflections, is nothing but the relative value of the integrated partial reflectivity.

4. Reflectivity of a plane infinite slab in reflection geometry

The unsymmetrical reflection case, for an infinite plane slab of thickness t is illustrated in Fig. 3 which is obtained from Fig. 2 by drawing in the crystal faces. χ_r denotes the angle between $\mathbf{n}_c$ (the inward normal of the crystal surface) and the normal to the most probable reflecting planes under consideration. γ_0 and γ_H are the direction cosines of $\mathbf{k}_I$ and $\mathbf{k}_F$ with respect to $\mathbf{n}_c$:

$$\gamma_0 = \sin(\theta_B - \chi_r),$$

$$\gamma_H = -\sin(\theta_B + \chi_r).$$

Remembering that $|\mathbf{k}_n\rangle$ denotes the initial wave-vector state of neutrons attaining the final $|\mathbf{k}_0\rangle$ state after n successive reflections, we write

$$(\mathbf{k}_{2j})_{\text{most probable}} = \mathbf{k}_F,$$

$$(\mathbf{k}_{2j+1})_{\text{most probable}} = \mathbf{k}_I. \quad (22)$$

The geometry of the problem allows us to use only one spatial coordinate, x, measured along $\mathbf{n}_c$. Then the linear coordinates of a certain point x, measured along $\mathbf{k}_{2j}$ or $\mathbf{k}_{2j+1}$, are given by

$$l_{2j}(x) = (x - t)/|\gamma_H|,$$

$$l_{2j+1}(x) = x/|\gamma_0|. \quad (23)$$

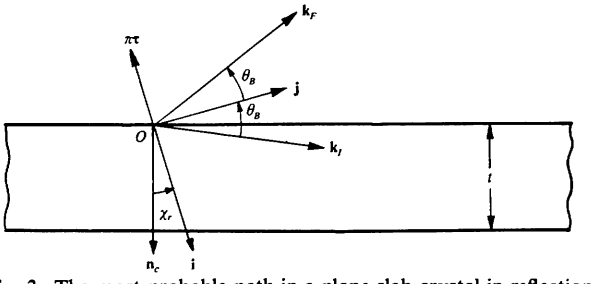

Fig. 3. The most probable path in a plane-slab crystal in reflection geometry.

In the general formulae of the previous sections every $\mathbf{r}_n$ is replaced by x_n, while

$$x_0 = 0$$

$$x_{2j,F} = t \; (j = 1, 2, \ldots),$$

$$x_{2j+1,F} = 0 (j = 0, 1, \ldots).$$

Then, from (11), (18) and (23),

$$R_{2j+1} = \frac{\mu_B^{2j+1}}{|\gamma_H^{j+1} \gamma_0^j| \alpha^{2j+1}} Y_{2j+1}(0, u_0), \qquad (24)$$

where

$$\alpha = \mu_T \left(\frac{1}{|\gamma_0|} - \frac{1}{|\gamma_H|} \right),$$

$$u_i = \alpha x_i \quad (i = 1, 2, \ldots), \qquad (25)$$

$$u_0 = \alpha t$$

and

$$Y_{2j+1}(u, u_0) = \int_u^{u_0} du_1 e^{-u_1} \int_0^{u_1} du_2 e^{u_2} \int_{u_2}^{u_0} du_3 e^{-u_3} \ldots$$

$$\ldots \int_0^{u_{2j-1}} du_{2j} e^{u_{2j}} \int_{u_{2j}}^{u_0} du_{2j+1} e^{-u_{2j+1}}.$$

From the above equation we can easily obtain the recurrence relation

$$Y_{2j+1}(u, u_0) = \int_u^{u_0} du' e^{-u'} \int_0^{u'} du'' e^{u''} Y_{2j-1}(u'', u_0) \qquad (26)$$

as well as

$$Y_1(u, u_0) = e^{-u} - e^{-u_0}.$$

In what follows we look for a solution of (26) of the following form:

$$Y_{2j+1}(u, u_0) = P_j(u) e^{-u} - P_j(u_0) e^{-u_0} + Q_j(u) - Q_j(u_0), \qquad (27)$$

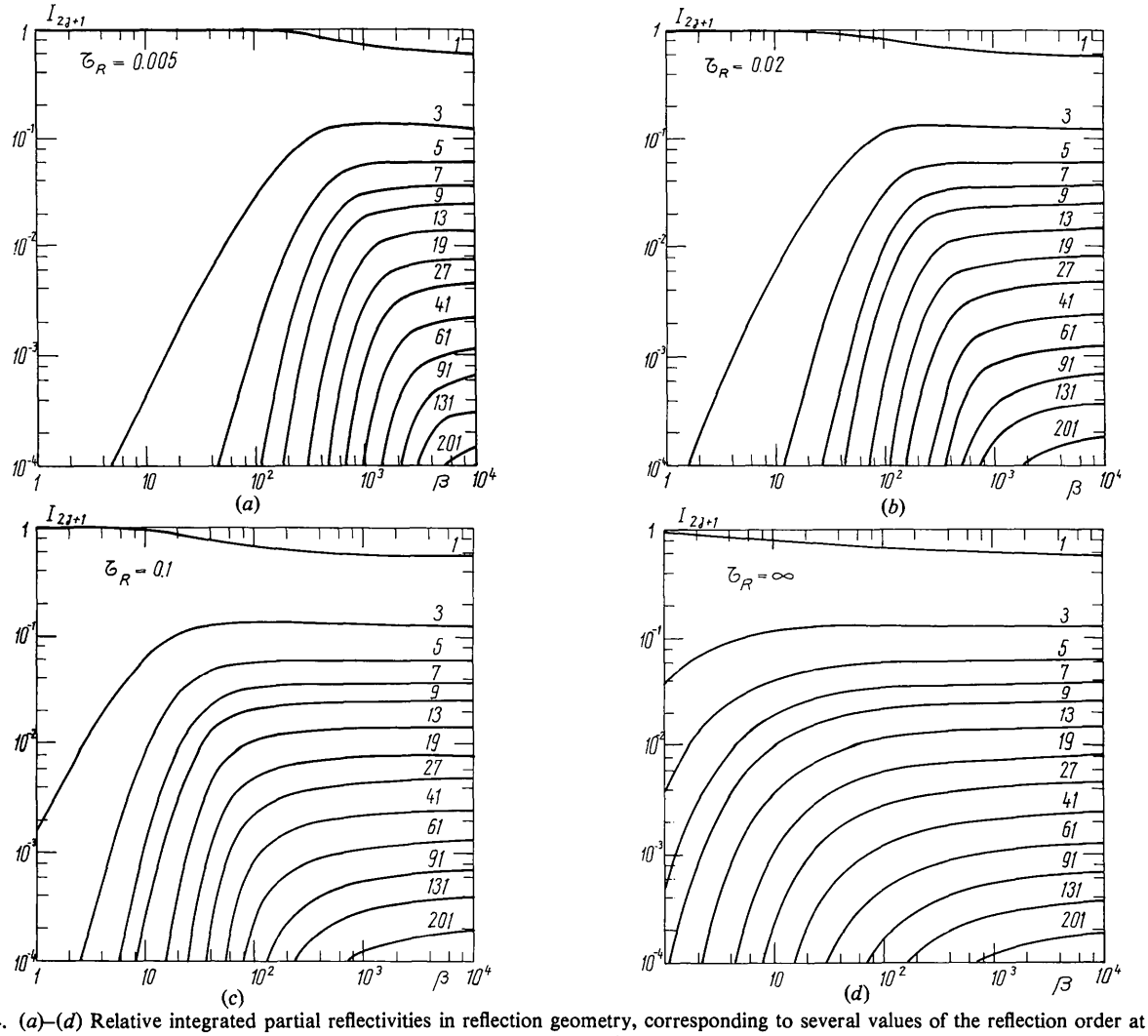

Fig. 4. (*a*)–(*d*) Relative integrated partial reflectivities in reflection geometry, corresponding to several values of the reflection order at a given relative thickness τ_R.

where

$$P_j(u) = \sum_{l=0}^{j} A_l^j u^l, \quad Q_j(u) = \sum_{l=0}^{j} B_l^j u^l, \tag{28}$$

with

$$A_0^1 = 1 \quad \text{and} \quad A_1^1 = B_0^1 = B_1^1 = 0.$$

Introducing (27) and (28) into (26), we get the following recurrence relations:

$$A_0^j = P_{j-1}(u_0)e^{-u_0} + Q_{j-1}(u_0) + \sum_{m=0}^{j-1} A_m^{j-1} m! - \sum_{m=0}^{j-1} (-1)^m B_m^{j-1} m!;$$

$$A_i^j = \sum_{m=0}^{j-i} \frac{(i+m-1)!}{i!} A_{i+m-1}^{j-1} \quad (i = 1, 2, \ldots);$$

$$B_0^j = 0; \tag{29}$$

$$B_1^j = P_{j-1}(u_0)e^{-u_0} + Q_{j-1}(u_0) - \sum_{m=0}^{j-1} (-1)^m B_m^{j-1} m!;$$

$$B_i^j = -\sum_{m=0}^{j-i} (-1)^m \frac{(i+m-1)!}{i!} B_{i+m-1}^{j-1} \quad (i = 2, 3, \ldots).$$

For $u_0 = \infty$ we assume the simple form:

$$Y_{2j+1}(u, \infty) = P_j(u)e^{-u}, \tag{30}$$

for which one obtains

$$A_i^j = (i+1)\frac{(2j-i)!}{i!(j-i)!\,(j+1)!}. \tag{31}$$

For the symmetric reflection ($\chi_r = 0$), introducing the notation:

$$t_R = \frac{\sin\theta_B}{\mu} = \text{penetration depth in the absence of Bragg scattering, in reflection geometry;}$$

$$\tau_R = t/t_R; \quad B = Q_c/\mu; \tag{32}$$

$$a = Bw_H(\xi); \quad \beta = Bw_H(0);$$

we get

$$u_0 = 2\tau_R(1+a) \tag{33}$$

and the reflectivity takes the following form:

$$R_{2j+1} = \left[\frac{a}{2(1+a)}\right]^{2j+1} Y_{2j+1}(0, u_0). \tag{34}$$

Figs. 4(*a*)–(*d*) illustrate I_{2j+1}, the relative values of the integrated partial reflectivities, *vs* β, for several values of the parameters τ_R. As expected, the greater the thickness of the crystal, the greater the amount of multiply reflected neutrons.

The mean number of reflections, defined by (21), is plotted in Fig. 5.

The calculations have been carried out with the help of an IBM 370/135 computer.

5. Reflectivity of a plane infinite slab in transmission geometry

Fig. 6 illustrates the case of unsymmetric transmission geometry. χ_t denotes the angle between $\mathbf{n}_c$ and the most probable reflecting planes.

The direction cosines of $\mathbf{k}_I$ and $\mathbf{k}_F$ are now given by

$$\gamma_0 = \cos(\theta_B - \chi_t),$$

$$\gamma_H = \cos(\theta_B + \chi_t). \tag{35}$$

Equations (22) and (25) are still valid, while

$$l_{2j}(x) = x/|\gamma_H| \quad (j = 0, 1, \ldots),$$

$$l_{2j+1}(x) = x/|\gamma_0| \tag{36}$$

and

$$x_0 = t, \quad x_{j,F} = 0. \tag{37}$$

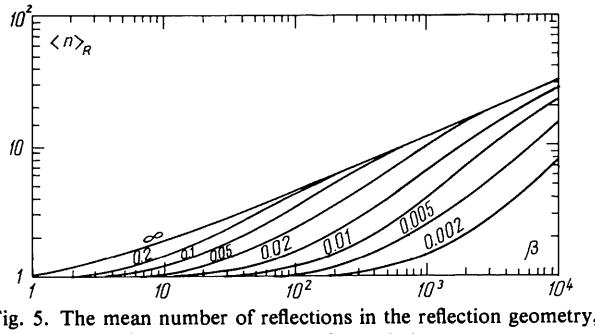

Fig. 5. The mean number of reflections in the reflection geometry, corresponding to several values of the relative thickness τ_R.

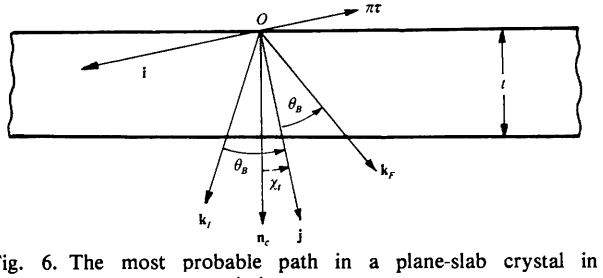

Fig. 6. The most probable path in a plane-slab crystal in transmission geometry.

Consequently, according to (11), (18) and (37), we obtain

$$R_{2j+1} = \frac{\mu_B^{2j+1} \exp(-\mu_T t/\gamma_H)}{|\gamma_H^{j+1} \gamma_0^j| \alpha^{2j+1}} Y_{2j+1}(u_0), \qquad (38)$$

where

$$Y_{2j+1}(u_0) = \int_0^{u_0} du_1\, e^{-u_1} \int_0^{u_1} du_2\, e^{u_2} \ldots$$
$$\ldots \int_0^{u_{2j-1}} du_{2j}\, e^{u_{2j}} \int_0^{u_{2j}} du_{2j+1}\, e^{-u_{2j+1}}. \qquad (39)$$

The case of unsymmetrical transmission is considered in Appendix *B*.

In the symmetrical geometry, $\alpha = 0$ and

$$R_{2j+1} = e^{-(\tau_T + y)} y^{2j+1}/(2j+1)!, \qquad (40)$$

where

$$y = a\tau_T, \quad \tau_T = t/t_T, \qquad (40')$$

$t_T = \cos\theta_B/\mu$ = penetration depth in the absence of Bragg scattering, in transmission geometry.

From (19) and (40) one obtains for the total reflectivity

$$R = e^{-(\tau_T + y)} \sinh y,$$

i.e. the expression given by Dietrich & Als-Nielsen (1965) for the symmetric case.

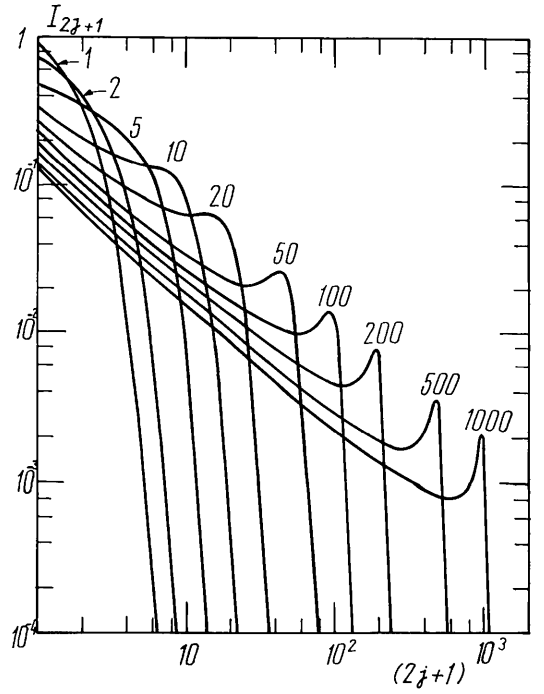

Fig. 7. Relative partial integrated reflectivities in transmission geometry *vs* reflecting order, corresponding to several values of y_0. Even if this function is defined only for odd-integer values on the abscissa, the points corresponding to the same y_0 are joined for the clearness of the diagram by a solid line.

The partial reflectivities have now some peculiar properties. So, as can be easily obtained from (40), when

$$2j + 1 < y_0 = \beta\tau_T,$$

the partial reflectivity is split with respect to the variable ξ, having two symmetric maxima for

$$\xi_{2j+1} = \pm \eta_H \left[2 \ln \left(\frac{y_0}{2j+1}\right)\right]^{1/2}.$$

When $2j + 1 > y_0$, the partial reflectivity is a clockwise function centered on $\xi = 0$, as well as the total reflectivity.

In Fig. 7 are shown I_{2j+1}, the integrated partial reflectivities, *vs* reflecting order, for several values of y_0. Even if these functions are defined only for odd-integer values on the abscissa, the points corresponding to the same y_0 are joined, for the clearness of the diagram, by a solid line. It is worth noting the presence of maxima in the dependency of integrated partial reflectivities on the reflecting order; the more pronounced, the greater the values of y_0.

In Fig. 8 is plotted, as a function of y_0, the mean number of reflections, given in this case by

$$\langle n \rangle_T = \int e^{-y} y \cosh y \, d\xi / \int e^{-y} \sinh y \, d\xi.$$

6. Vertical broadening of the beam. Neutron leakage

It follows from (15) that, in the case of a vertically collimated incoming beam, the distribution function of the vertical divergence angles of $(2j + 1)$-times reflected neutrons is given by

$$v_{2j+1}(\delta_0) = \beta_0[\beta_0^2 + 4(2j+1)\eta_V^2 \sin^2\theta_B]^{-1/2}$$
$$\times \exp\{-\delta_0^2/[2\beta_0^2 + 8(2j+1)\eta_V^2 \sin^2\theta_B]\} \qquad (41)$$

so that

$$\Phi[l_0(\mathbf{r}_0)]v(\delta_0) = \sum_{j=0}^{\infty} \Phi_{2j+1}[l_0(\mathbf{r}_0)]v_{2j+1}(\delta_0). \qquad (42)$$

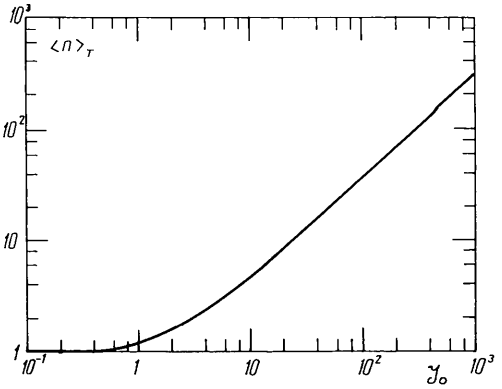

Fig. 8. The mean number of reflections in the transmission geometry.

Assuming that $v(\delta_0)$ is a Gaussian distribution, from (41), (42) and the definition of the mean number of reflections, $\langle n \rangle$, we obtain

$$v(\delta_0) = \beta_0[\beta_0^2 + 4\langle n \rangle \eta_V^2 \sin^2 \theta_B]^{-1/2} \times \exp\{-\delta_0^2/[2\beta_0^2 + 8\langle n \rangle \eta_V^2 \sin^2 \theta_B]\}. \quad (43)$$

Hence, the multiple Bragg reflections induce, when $\langle n \rangle$ takes large values, a pronounced vertical broadening of the diffracted beam, accompanied by a complementary diminution of $v(0)$.

A wavelength-dependent 'effective vertical mosaic spread' of the crystal may be defined by

$$\eta_V^{\text{eff}} = \sqrt{\langle n \rangle}\, \eta_V. \quad (44)$$

This is the quantity which must be used instead of η_V in calculating the resolution function of crystal spectrometers.

In order to estimate how important the vertical broadening is likely to be quantitatively, we have calculated the ratio between the instrumental intensity obtained for several values of $\langle n \rangle$ and that corresponding to $\langle n \rangle = 1$, when this effect is neglected. For a triple-axis neutron spectrometer, with a double-crystal monochromator unit, in an elastic-diffraction set-up, in the case of a cross section (and resolution function) isotropic in **Q**-space this ratio is given by (Grabcev, 1973)

$$\frac{I_n}{I_1} = \left[\frac{(c^2+1)(2c^2+1)}{(c^2+\langle n \rangle)(2c^2+\langle n \rangle)}\right]^{1/2}, \quad (45)$$

where

$$c = \beta_0/2\eta_V|\sin \theta_B|.$$

We have assumed identical single crystals and vertical collimation angles.

In Fig. 9 I_n/I_1 is shown, calculated as a function of $\langle n \rangle$, for several values of the parameter c. Taking into account that values of c of about 1 and of $\langle n \rangle$ greater than 2 are usual, we conclude that the neutron leakage caused by the vertical broadening of the reflected beam may involve important losses of experimental intensity. This is in agreement with the results of Riste (1970) and Nunes & Shirane (1971), who by using vertically bent crystals have compensated for the vertical broadening (or a part of it) by spatial focusing, attaining essential gains of luminosity. The neutron leakage is expected to be very pronounced in back-reflection spectrometers.

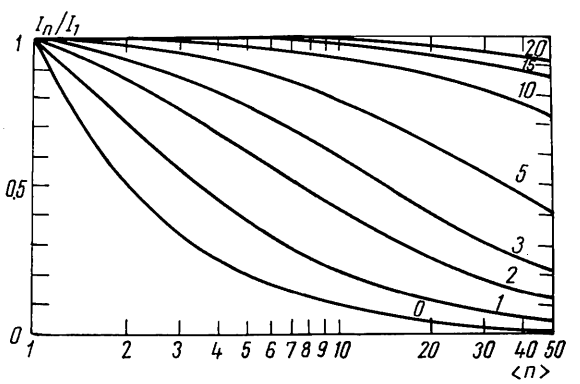

Fig. 9. Diagram illustrating the neutron leakage caused by multiple Bragg reflections in monochromator and analyzer crystals of a triple-axis spectrometer.

7. Experimental results. Discussion

The mean number of reflections may be determined experimentally from the width of a vertical scanning, performed by rotating the crystal about the horizontal **j** axis contained in the reflecting plane (Fig. 2), in a white neutron beam.

It is easy to show that when ψ_1 is the vertical missetting angle, the vertical divergence angle of a reflected neutron becomes

$$\delta_0' = \delta_0 - 2\psi_1 \sin \theta_B.$$

Therefore, if β_0 and β_1 are the vertical collimation angles of the collimators defining the incoming and reflected beams, taking into account (43) we obtain for the intensity of a vertical scan the following equation:

$$I(\psi_1) \simeq \int v(\delta_0 - 2\psi_1 \sin \theta_B) \exp(-\delta_0^2/2\beta_1^2)\, d\delta_0 = \sqrt{2\pi}\beta_0\beta_1[\beta_0^2 + \beta_1^2 + 4\langle n \rangle \eta_V^2 \sin^2 \theta_B]^{-1/2} \times \exp\{-4\psi_1^2 \sin^2 \theta_B \times [2\beta_0^2 + 2\beta_1^2 + 8\langle n \rangle \eta_V \sin^2\theta_B]^{-1}\}. \quad (46)$$

Introducing widths instead of standard deviations, *i.e.*

$$b_i = \sqrt{8 \ln 2}\, \beta_i \quad \text{and} \quad m_V = \sqrt{8 \ln 2}\, \eta_V,$$

the width of a vertical scan is given by

$$l = [l_0^2 + \langle n \rangle m_V^2]^{1/2}, \quad (47)$$

where

$$l_0 = \frac{(b_0^2 + b_1^2)^{1/2}}{2|\sin \theta_B|}$$

is the resolution width of the experimental set-up. It may be measured with a perfect crystal.

In order to obtain a suitable value of l_0 we have put $b_0 = b_1 = 10'$ and have performed the measurements of the vertical scans at large Bragg angles.

The experimental values of $\langle n \rangle$ obtained for Cu(111), Zn(002) and Pb(111) single crystals, in symmetric reflection geometry, are compared with theoretical values, $\langle n \rangle_{\text{theor.}}$, in Table 1. Besides crystal thickness and horizontal mosaic spread, the reflectivity is defined in terms of intrinsic material parameters B, t_R and t_T from (32) and (40′). In calculating $\langle n \rangle_{\text{theor.}}$ we have used the wavelength-dependent values of B and t_R

Table 1. *The experimental values of the mean number of reflections obtained from the widths of vertical scans in reflection geometry.*

The relative errors are about 5%. $\langle n\rangle_{\text{theor.}}$ has been calculated within the infinite geometry model.

Crystal	λ (Å)	$\langle n\rangle_{\text{exp.}}$	$\langle n\rangle_{\text{theor.}}$
Cu(111)	2·92	1·4	2·6
145 × 52 × 100 mm	3·17	1·6	2·8
	3·37	1·9	3·1
	3·52	2·3	3·5
	3·75	2·7	4·9
Zn(002)	2·02	1·5	2·1
10 × 65 × 142 mm	3·46	2·5	3·6
	3·80	2·8	4·0
	4·05	2·9	4·2
	4·28	3·2	5·0
Pb(111)	2·85	1·5	2·8
11 × 60 × 163 mm	4·47	3·6	4·9
	4·81	3·9	6·1
	5·13	4·3	7·2

defined in terms of experimentally determined μ (Grabcev, 1979).

We can see in Table 1 that, as well as in the case of experimental determination of peak and integrated reflectivities (Popovici, Gheorghiu & Gelberg, 1969; Dorner, 1971; Malik, 1976), the experimental values of $\langle n\rangle$ are smaller than those predicted by theory. These differences are partially explained by the fact that experiments are carried out with finite beams and bounded crystals while the theoretical values are calculated within the infinite geometry.

Nevertheless, the customary model of infinite plates is largely used in the literature in analyzing the crystal reflectivity because it provides analytical solutions easy to handle with transparent physical meaning. That is why, in order to outline the salient features of multiple Bragg reflections, we have preferred to use this model, the calculation of the exact numerical value of $\langle n\rangle$ for a certain experimental situation being beyond the scope of the present paper.

In particular cases with finite geometries our method is similar to that of Werner, Arrott, King & Kendrick (1966), but taking into account at the same time the vertical divergence angles and mosaic spread.

Concluding remarks

The general method presented in § 2 may be applied in analyzing the multiple-scattering effects for any scattering cross section and for any sample geometry. In the particular case of elastic coherent scattering it closely parallels that of Werner & Arrott (1965).

In any case, when single crystals are used as samples in neutron-diffraction experiments, the calculation method may be applied to include vertical broadening in the corrections for secondary extinction.

It has been shown that the crystal reflectivity depends only on the horizontal mosaic spread, while the vertical mosaic spread determines solely the distribution of vertical divergence angles in the diffracted beam.

Beyond the rather academic interest for comparing relative reflectivities in terms of reflecting orders, we succeeded in calculating the mean number of reflections defining the effective vertical mosaic spread of the crystal, and from this the resolution function of crystal spectrometers.

The present paper provides supplementary arguments to support Freund's (1975) proposal concerning the use of single-crystal monochromators with anisotropic mosaic structure: a suitable horizontal mosaic spread will ensure the most convenient compromise between resolution and intensity while a small vertical mosaic spread will avoid an exaggerated broadening of the reflected beam.

APPENDIX *A*

Elastic-coherent-scattering cross section of mosaic crystals

The elastic-coherent-scattering cross section of perfect crystals is given by (Cassels, 1950)

$$\frac{\mathrm{d}\mu_{Bp}}{\mathrm{d}\mathbf{k}_f}=\frac{(2\pi)^3|F|^2}{V_c^2k_i^2}\sum_{\tau}\delta(\mathbf{Q}+2\pi\tau)\delta(k_i-k_f), \quad (A1)$$

where F is the structure factor squared times the Debye–Waller factor and V_c is the volume of a unit cell; $\mathbf{Q}=\mathbf{k}_i-\mathbf{k}_f$ is the scattering vector.

In the reference frame illustrated in Fig. 2, in which a certain reciprocal vector of the most probable mosaic blocks ($\varphi=\psi=0$) is in the opposite direction to the $\mathbf{i}$ axis (*i.e.* $\tau=-\tau\mathbf{i}$), the corresponding reciprocal vector attached to a mosaic block, described by the horizontal and vertical mosaic angles φ and ψ, respectively, is expressed as

$$\boldsymbol{\tau}=-\tau\mathbf{i}-\tau\varphi\mathbf{j}+\tau\psi\mathbf{k}. \quad (A2)$$

If Q_1, Q_2 and Q_3 are the Cartesian components of $\mathbf{Q}$,

$$Q_1=2k_i\sin\theta_B+(\gamma_f-\gamma_i)k_I\cos\theta_B,$$

$$Q_2=k_I(\gamma_i+\gamma_f)\sin\theta_B,$$

$$Q_3=k_I(\delta_i-\delta_f),$$

from (*A*1) and (*A*2),

$$k_f=k_i=k_I[1+(\gamma_i-\varphi)\cot\theta_B], \quad (A3)$$

$$\gamma_f=2\varphi-\gamma_i, \quad (A4)$$

$$\delta_f=\delta_i+2\psi\sin\theta_B. \quad (A5)$$

The elastic-coherent-scattering cross section of mosaic crystals is found by averaging (*A*1) with respect to the mosaic block distribution, *i.e.*

$$\frac{\mathrm{d}\mu_B}{\mathrm{d}\mathbf{k}_f} = \int \frac{\mathrm{d}\mu_{Bp}}{\mathrm{d}\mathbf{k}_f} w_H(\varphi) w_V(\psi)\, \mathrm{d}\varphi\, \mathrm{d}\psi.$$

Hence, when the distribution functions $w_H(\varphi)$ and $w_V(\psi)$ are Gaussians,

$$w_H(\varphi) = (1/\sqrt{2\pi}\eta_H) \exp(-\varphi^2/2\eta_H^2)$$

and

$$w_V(\psi) = (1/\sqrt{2\pi}\eta_V) \exp(-\psi^2/2\eta_V^2),$$

the scattering cross section becomes

$$\frac{\mathrm{d}\mu_B}{\mathrm{d}\mathbf{k}_f} = \frac{Q_c}{\sqrt{2\pi}\eta_H} \frac{1}{k_I^2} \frac{1}{\sqrt{8\pi}\eta_V |\sin\theta_B|} \times \exp\left[-\frac{(\gamma_I+\gamma_f)^2}{8\eta_H^2}\right] \exp\left[-\frac{(\delta_I-\delta_f)^2}{8\eta_V^2 \sin^2\theta_B}\right] \times \delta(k_I - k_f)\, \delta\left(\gamma_f - \gamma_I + 2\frac{k_I - k_I}{k_I}\tan\theta_B\right), \tag{A6}$$

where

$$Q_c = \frac{(2\pi)^3 |F|^2}{V_c^2 k_I^3 |\sin 2\theta_B|}. \tag{A7}$$

Q_c is proportional to the total macroscopic elastic-coherent-scattering cross section of single crystals. So, for a perfect crystal

$$\mu_{Bp} = Q_c \delta(\xi),$$

while for a mosaic crystal

$$\mu_B = Q_c w_H(\xi), \tag{A8}$$

where

$$\xi = \gamma_I - \frac{k_i - k_I}{k_I}\tan\theta_B. \tag{A9}$$

APPENDIX *B*

The unsymmetrical transmission case

From (39) we can deduce the recurrence relation

$$Y_{2j+1}(u) = \int_0^u \mathrm{d}u'\, e^{-u'} \int_0^{u'} \mathrm{d}u''\, e^{u''}\, Y_{2j-1}(u'') \tag{B1}$$

and

$$Y_1(u) = 1 - e^{-u}.$$

We try to find for (*B*1) solutions of the form

$$Y_{2j+1}(u) = P_j(u)\, e^{-u} + Q_j(u),$$

where $P_j(u)$ and $Q_j(u)$ are polynomials as in (28). Introduction of these into (*B*1), after integration, results in the following recurrence relations for the coefficients:

$$A_0^j = -\sum_{m=0}^{j-1} A_m^{j-1} m! + \sum_{m=0}^{j-1} (-1)^m B_m^{j-1} m!;$$

$$A_i^j = -\sum_{m=0}^{j-i} \frac{(i+m-1)!}{i!} A_{i+m-1}^{j-1} \quad (i = 1, 2, \ldots);$$

$$B_0^j = \sum_{m=0}^{j-1} A_m^{j-1} m! - \sum_{m=0}^{j-1} (-1)^m B_m^{j-1} m!;$$

$$B_i^j = \sum_{m=0}^{j-i} (-1)^m \frac{(i+m-1)!}{i!} B_{i+m-1}^{j-1}.$$

From the above equations we find, by complete induction, the following relations:

$$A_i^j = (-1)^{j+1} \frac{(2j-i)!}{i!(j-i)!\, j!};$$

$$B_i^j = (-1)^{j-i} \frac{(2j-i)!}{i!(j-i)!j!}.$$

References

BACON, G. E. & LOWDE, R. D. (1948). *Acta Cryst.* **1**, 303–314.

BECKER, P. J. & COPPENS, P. (1974). *Acta Cryst.* A**30**, 129–153.

CASSELS, J. M. (1950). *Prog. Nucl. Phys.* **1**, 185–215.

DIETRICH, O. W. & ALS-NIELSEN, J. (1965). *Acta Cryst.* **18**, 184–188.

DORNER, B. (1971). *J. Appl. Cryst.* **4**, 185–189.

FREUND, A. (1975). *Nucl. Instrum. Methods*, **124**, 93–99.

GRABCEV, B. (1973). *Rev. Roum. Phys.* **18**, 373–379.

GRABCEV, B. (1979). *Reflecting Properties of Some Neutron Monochromators*. Report IRNE-133, Institute of Nuclear Power Reactors, Pitesti.

MALIK, S. S. (1976). *J. Appl. Cryst.* **9**, 273–278.

NUNES, A. C. & SHIRANE, G. (1971). *Nucl. Instrum. Methods*, **95**, 445–452.

POPOVICI, M., GHEORGHIU, Z. & GELBERG, D. (1969). *Nucl. Instrum. Methods*, **69**, 125–130.

RISTE, T. (1970). *Nucl. Instrum. Methods*, **86**, 1–4.

SEARS, V. F. (1975). *Adv. Phys.* **24**, 1–45.

WERNER, S. A. & ARROTT, A. (1965). *Phys. Rev.* **140**, A675–A686.

WERNER, S. A., ARROTT, A., KING, J. S. & KENDRICK, H. (1966). *J. Appl. Phys.* **37**, 2343–2350.